Carbon 211 (2023) 118100

Contents lists available at ScienceDirect

Carbon

journal homepage: www.elsevier.com/locate/carbon

One-step synthesis of MN_4 molecular electrocatalysts assembled on different nanocarbon architectures for efficient oxygen reduction

Alicia Trigueros-Sancho [a], Beatriz Martínez-Sánchez [a,*], Diego Cazorla-Amorós [b], Emilia Morallón [a,**]

[a] Departamento de Química Física and Instituto Universitario de Materiales de Alicante (IUMA), University of Alicante, Ap. 99, 03080, Alicante, Spain
[b] Departamento de Química Inorgánica and Instituto Universitario de Materiales de Alicante (IUMA), University of Alicante, Ap. 99, 03080, Alicante, Spain

ARTICLE INFO

Keywords:
One-step synthesis
Solvent-free ball-milling
Mechanochemistry
Carbon materials
Iron and cobalt phthalocyanines
Oxygen reduction reaction
Electrocatalysis
Precious metal-free catalyst

ABSTRACT

One-step dry ball-milling method was employed to prepare different electrocatalysts based on cobalt(II) or iron (II) phthalocyanines (CoPc and FePc, respectively) supported on commercial carbon materials (CNovel or a carbon black (Vulcan)), controlling the nominal metal content to 1 or 2 wt %. No pre-treatment (e.g., functionalization of the carbon support), solvent addition or post-processing steps (e.g., heat-treatment, acid-treatment, etc.) were required before, during or after the mechanochemical process. Different characterization techniques have been used to study the morphological, physicochemical and electrochemical properties of the synthesized materials. The as-prepared catalysts can be directly used without involving further procedure. Solid-state ball-milling strategy provides excellent contact of both components, which synergistically improved their electrocatalytic performance. Regarding the carbon materials, the adequate nanoarchitecture and surface chemistry of CNovel permits better distribution of metal phthalocyanines (MPc) compared to a carbon black. The FePc supported on CNovel shows excellent electrocatalytic activity for oxygen reduction reaction (ORR), in terms of good selectivity towards the 4-electron pathway, long-term stability and low overpotential in alkaline medium. This study opens new paths for a simple, scalable and cost-effective catalyst manufacturing through mechanochemistry that can be modulated by selecting the proper nanocarbon support and MPc/carbon ratio.

1. Introduction

Oxygen reduction reaction (ORR) is a well-known cathodic reaction that takes place in many electrochemical energy generation devices, such as fuel cells or metal-air batteries [1–3], in which platinum (Pt)-based materials are normally used as catalysts due to their high catalytic activity and chemical stability [4]. However, high Pt loadings are required to overcome the kinetic limitations of the ORR, which entails high costs, together with other important drawbacks such as the shortage, poisoning deactivation or dissolution/aggregation under acidic and oxidizing conditions [5]. Therefore, alternative materials are highly needed to replace the precious metal in Pt-based electrocatalysts, looking for the best characteristics in terms of low-cost, good efficiency, high surface area and porous structure to host numerous active sites, good electrical conductivity and electrochemical stability [6].

Metal-N_4 complexes (MN_4) (typically, M = Co or Fe) [7–9] have been deeply used in many research studies since the 1960s [10], when both metal porphyrins (MPy) and phthalocyanines (MPc) were found to exhibit good ORR performance, especially in alkaline medium. Their high catalytic activity is mainly related to the conjugated 4-fold *N*-coordination surrounding of the central metal atom [11], where the nature of the metal and the presence of peripheral or non-peripheral substitution in the phthalocyanine play a crucial role in their activity [12]. Moreover, the growing interest of MPc lies in their high performance and selectivity, low cost, chemical and thermal stability, straightforward large-scale production, high versatility and easy functionalization [13,14]. Owing to their successful application in ORR, these molecules have also attracted substantial attention in other electrocatalytic reactions, such as carbon dioxide reduction reaction (CO_2RR) [15,16], oxygen evolution reaction (OER) and hydrogen evolution reaction (HER) [17,18], which are essential for sustainable energy technologies. However, one of their main drawbacks is their both poor stability and electrical

* Corresponding author.
** Corresponding author.
E-mail address: beatriz.ms@ua.es (B. Martínez-Sánchez).

https://doi.org/10.1016/j.carbon.2023.118100
Received 10 March 2023; Received in revised form 9 May 2023; Accepted 10 May 2023
Available online 10 May 2023

conductivity [8,19]. Additionally, aggregation of MPc molecules leads to eventual loss of the catalytic activity in practical applications [20], which makes necessary to disperse and support them on highly conductive surfaces for a better performance. In this sense, strong interactions between the catalyst and the support are key, not only to increase the electron transfer in the electrocatalytic process, but also to enhance the catalytic performance and reduce the catalyst loss [13].

Then, the incorporation of conductive carbon supports forming MPc/carbon composites has improved the catalytic properties, as consequence of the increase in the dispersion of active sites, together with an improved charge transport [13]. Interestingly, Yang et al. [21] demonstrated the relevance of selecting the carbon support for improving the ORR performance and the long-term durability of the MPc/carbon composites. Carbon materials, such as carbon blacks, graphene or carbon nanotubes (CNTs), have been widely studied for electrochemical applications like hydrogen storage, sensors or as electrocatalyst supports, due to their accessibility, relatively low cost, environmental compatibility, different nanostructures, and excellent electrical conductivity and mechanical properties [22–24]. Moreover, there is a growing interest in other micro and mesoporous nanostructured carbon materials that facilitate the diffusion of reactants and products, along with an increase in the interaction with the catalyst [25,26]. Here, CNovel is a new carbon nanomaterial based on hollow nanospheres with interconnected mesopores that can be used not only as adsorbent or in analytical instrumentations, but also in other applications as energy storage and renewable/conversion technologies [27]. Interestingly, both the pore size and particle size distribution can be precisely controlled by selecting the size of the template in the synthesis process [28]. However, few works can be found [29–32] in which CNovel is used as catalyst support. Here, Pt nanoparticles and Pt@Pd core-sell catalysts were mainly employed as the active phase. Therefore, CNovel arises as a promising mesoporous carbon that needs to be further exploited as molecular catalyst support.

To date, multiple approaches have been studied for the preparation of carbon-based electrocatalysts [33], both free and metal-containing catalysts, including different physical [34–37], thermo-chemical [38–40] and electrochemical processes [41–43], among many others. For example, sonication of chemically modified FePc with oxidized CNTs was used for the synthesis of well-dispersed molecular catalysts with high ORR activity and stability in alkaline medium [44]. Other synthetic strategy reported by Yoshii et al. was the controlled incorporation of MN_4 sites embedded into ordered porous carbon frameworks by structure-preserving carbonization via solid-state polymerization [45]. Within all these methods, some strategies such as heteroatom doping, surface functionalization, edges and defects engineering, etc. can be used to increase the catalytic performance of carbon materials [33]. Nonetheless, most of these synthesis procedures show some problems in terms of the low yield and the use of pollutant and harmful reagents [46]. Then, the ball-milling method has been positioned as a powerful green mechanochemical synthesis alternative [47] in which the kinetic energy produces nanostructured materials by activating chemical reactions, modifying the reactivity of as-milled materials and inducing phase changes [46,48], avoiding the generation of residues and the use of large amounts of solvents. Moreover, the ball-milling process has been reported not only for solid-solid reactions, but also for solid-liquid and solid-gas reactions [46], by selecting the operating conditions (temperature, milling time, rotation rate, reagents, etc.). Furthermore, ball-milling conditions can be controlled to produce edge-functionalized or edge-doped carbon-based nanocatalysts maintaining the carbon structure [49], which are well-known to be highly active and stable towards the ORR. In addition, ball-milling has also been used to improve the interaction in different metal/carbon composites and to enhance the electrocatalytic activity [46,50–52]. For example, Karuppiah et al. [53] prepared a bifunctional catalyst for ORR and OER, where cobalt oxide nanospheres were dry ball-milled together with carbon black and $LaMnO_3$ perovskite.

Nonetheless, most of reported works combined ball-milling with other procedures; in particular, Wang et al. [48] obtained Co-containing composites by ball-milling and subsequent heat-annealing as promising electrocatalysts towards the ORR in alkaline medium. Moreover, Costa de Oliveira et al. [54] combined dry impregnation, ball-milling process and pyrolysis treatments in the presence of iron phthalocyanines (FePc), urea and carbon black to obtain Fe–N–C catalysts with enhanced ORR activity and stability in neutral medium. Wang et al. [55] also reported a combined preparation method of ball-milling with an additional pyrolysis treatment, leading to Co nanoparticles on C–N nanosheets with good catalytic performance in a wide pH range. Other works have also focused on the preparation of Co–N–C catalysts by following similar strategies [56]. Interestingly, ball-milling has been reported to promote stronger intermolecular π-π interactions and good MPc distribution in metal phthalocyanines on carbon materials [52,54]. In addition, low temperatures prevent the structural damage of MN_4 complexes. In all cases, the role of ball-milling is to highlight the contact of all the materials by mechanochemical mixing and to enhance the electrocatalytic activity due to synergy processes. Indeed, previous works from our research group [35,57] demonstrated the poor stability obtained by a simple wet impregnation of MPc on carbon nanotubes (CNTs), where a previous electrochemical functionalization of CNTs or post heat-treatment were required to enhance their interaction and their electrocatalytic performance towards ORR. Interestingly, Dodelet et al. published several works few years ago [58–61] in which ball-milling combined with pyrolysis treatments in presence of different Fe-precursors and NH_3 leads to enhanced Fe/N/C-catalysts for PEMFC. Nonetheless, few works [52,62] have been found in the literature in which the ball-milling process is used with metal phthalocyanines and carbon materials without any additional treatment, but the addition of solvent is normally required. This implies subsequent drying and grinding steps. From the best of our knowledge, the direct mechanochemical preparation of efficient molecular catalysts (MPc) on carbon materials via one-step dry ball-milling has not been reported before.

Then, in this work a straightforward and direct solvent-free ball-milling method in ambient conditions has been used to prepare cobalt (II) and iron(II) phthalocyanines (CoPc and FePc, respectively) supported on commercial carbon materials (carbon black Vulcan XC-72R and CNovel) as electrocatalysts for ORR in alkaline medium. The MPc/carbon composite materials have been characterized using different techniques (XPS, XRD, cyclic voltammetry, etc.) and their electrochemical activity towards ORR has been studied. This single-step mechanochemical synthesis strategy has great prospects in heterogeneous catalysis because of its ease and cost-effective scale-up for practical industrial production.

2. Experimental

2.1. Materials and reagents

The carbon materials used as supports were the commercial Vulcan® XC-72R carbon black (Vulcan) from Cabot Corporation and CNovel™ (MJ(4)150) supplied by Toyo Tanso, and they are used without further purification. Iron(II) phthalocyanine (FePc, 90%) and cobalt(II) phthalocyanine (CoPc, 97%), as well as platinum supported on a graphitized carbon material (20 wt % Pt) were used as received from Sigma-Aldrich. Nafion® was supplied by Sigma-Aldrich. Isopropanol (iPrOH) (C_3H_8O, 99.5%) and potassium hydroxide (KOH, 85%) were purchased from VWR Chemicals. Hydrochloric acid (HCl, 37%) and nitric acid (HNO_3, 65%) are purchased from PanReac AppliChem (ITW Reagents). All aqueous solutions were prepared with ultrapure water (18.2 MΩ cm, Millipore® Milli-Q® water). Nitrogen gas (N_2, 99.999%), oxygen gas (O_2, 99.995%) and hydrogen gas (H_2, 99.999%) were supplied by Carburos Metálicos.

2.2. Synthesis procedure

The iron and cobalt-based samples were mechanochemically prepared using the ball-milling method at room temperature and ambient atmosphere (see Scheme S1). Briefly, an appropriate amount of the carbon support (Vulcan or CNovel) and the M-phthalocyanine (CoPc or FePc) (total amount of 1 g) were ball-milled with 10 agate balls (10-mm diameter) in a Planetary Ball Miller PM 200 for several cycles of 30 min milling and 15 min pause with a rotation speed of 500 rpm, where the direction of rotation is reversed every cycle to ensure proper mixing of the precursors and to avoid high temperatures that could damage the well-defined molecular structure of MPc on carbon supports. This program is done during 4 h and 30 min. The volume of the agate ball-mill jar is 50 mL. The sample to ball mass ratio is 1:13.8 and the ball to jar volume ratio is about 1:9. Eight different samples were obtained with a nominal metal loading of 1 and 2 wt % and labelled as CNovel_M_wt% and Vulcan_M_wt% (M = Co or Fe). Table S1 includes the yield and nominal composition of catalysts. The mass required of CoPc and FePc have been calculated for each sample according to their molecular weight (571.5 g mol^{-1} and 568.4 g mol^{-1} for CoPc and FePc, respectively), the atomic weight of the corresponding metal (58.93 g mol^{-1} and 55.85 g mol^{-1} for Co and Fe, respectively) and their purity (97% and 90% for CoPc and FePc, respectively). The table also includes the yield of the ball milling process for the carbon materials without metal phthalocyanines for comparison purposes (Vulcan_m and CNovel_m, respectively). These yield values correspond to the amount of sample recovered after the milling.

2.3. Morphological and physico-chemical characterization

The morphology and microstructure of the samples were investigated by transmission electron microscopy (TEM) and scanning electron microscopy (SEM). TEM images were taken with a JEOL JEM-2010 model, INCA Energy TEM 100 model microscope with an electron beam of 200 keV, equipped with a GATAN brand model ORIUS SC600 acquisition camera. It is mounted in axis with the microscope at the bottom and is integrated into the GATAN Digital Micrograph 1.80.70 acquisition and processing program for GMS 1.8.0. This TEM microscope has a point-to-point resolution of 0.19 nm. The SEM microscope (Hitachi S–3000 N) is equipped with a brand Bruker model XFlash 3001 X-ray detector for microanalysis (EDX) and mapping. This equipment has a resolution of 3.5 nm in vacuum. Regarding sample preparation, homogeneous suspensions in isopropanol were dropped onto a copper grid and then completely dried before measurements.

The textural properties of materials were determined by adsorption-desorption of N_2 at −196 °C in an automatic volumetric adsorption equipment (Autosorb-6, Quantachrome, USA). For this purpose, 100 mg of dry sample was previously out-gassed at 250 °C under vacuum for 4 h. The apparent specific surface area was calculated from N_2 adsorption data by applying the Brunauer-Emmett-Teller (BET) equation [63] in the relative pressure range from 0.05 to 0.3. The total micropore volume (V_{DR}) was calculated using the Dubinin-Radushkevich (DR) equation to the N_2 adsorption in the low relative pressures region ($P/P_0 < 0.1$).

Structural information was also obtained by X-ray diffraction (XRD) using a Panalytical Empyrean equipment that has a goniometer with an X-ray tube with a Cu Kα cathode as the radiation source and a PIXcel 3D detector. The measurements were performed at a voltage of 40 kV and current of 40 mA. The step angle was 0.05° in the 2θ range from 10° to 80° and at room temperature.

The surface composition of the samples was measured by X-ray photoelectron spectroscopy (XPS) with a VG-Microtech Multilab 3000 spectrometer equipped with a semispherical electron analyzer with 9 channeltrons (passing energy of 2–200 eV) and an X-ray source with Al radiation (Kα 1253.6 eV). The binding energy scale was referenced to the main C1s signal, which was fixed at 284.6 eV. The samples were previously dried in vacuum.

Inductively Coupled Plasma Optical Emission Spectroscopy (ICP-OES) was employed for quantitatively determine the metal content of the prepared samples. The ICP-OES equipment used in this study was the PerkinElmer brand Optima 4300 DV (with dual vision). The preparation of the samples consists in diluting 25 mg of the metal containing samples in 2 mL of an acid solution ($HCl:HNO_3$ = 3:1, molar ratio) and stirring for 48 h. Afterwards, the sample was filtered with 0.45 μm filters and diluted to 25 mL with ultrapure water.

Temperature programmed desorption (TPD) experiments provide information about the nature and amount of surface functional groups of carbon material. TPD measurements were performed in a DSC-TGA system (SDT Q600 Simultaneous, TA Instruments, USA) coupled to a mass spectrometer (HiCube 80 Eco, Pfeiffer Vacuum, Germany). The sample (8–10 mg) was heat treated up to 950 °C (heating rate 20 °C min^{-1}), after a previous drying step at 120 °C for 30 min, under a helium flow rate of 100 mL min^{-1}. The mass loss is represented as a percentage with respect to the initial value, in each case, which corresponds to 100%. Amounts of CO and CO_2 desorbed from the sample, among other relevant signals, were monitored and quantified by a previous calibration using calcium oxalate. The desorbed gases are related to the decomposition of surface functional groups of the samples and to the reactions between the metal phthalocyanines and the carbon material.

2.4. Electrochemical characterization

Electrochemical characterization of the samples was performed in a three-electrode cell at 25 °C and using an Autolab PGSTAT302 with a dual mode bipotentiostat module (Metrohm, Netherlands). A rotating ring-disk electrode (RRDE, Pine Research Instruments, USA), equipped with a glassy carbon disk (5.61 mm diameter, 0.25 cm^2) and a Pt ring (0.19 cm^2) as working electrode (WE), was used. The WE was carefully polished with alumina slurries and rinsed with ultrapure water. A graphite bar (supplied by Mersen Ibérica) and a home-made reversible hydrogen electrode (RHE) immersed in the same electrolyte in a Luggin capillary were used as a counter and reference electrodes, respectively.

The WE was prepared by dropping a 1 mg mL^{-1} dispersion of the catalysts ink containing Fe and Co-based samples in an aqueous solution (20 vol % isopropanol, 76 vol % water and 4 vol % Nafion®). The dispersion was previously homogenized via ultrasonication for at least 30 min. Here, it is important to know the appropriate volume ratio that guarantees the perfect adhesion of the material. The amount of catalyst loading on the disk electrode was optimized in 0.48 mg cm^{-2}.

Cyclic voltammetry of the different electrocatalysts was performed in 0.1 M KOH N_2-saturated solution. The ORR was studied by linear sweep voltammetry (LSV), from 1.0 V to 0 V at scan rate of 5 mV s^{-1} in 0.1 M KOH O_2-saturated solution at six different rotation rates between 400 and 2025 rpm. In addition, a commercial 20 wt % Pt/C (Sigma -Aldrich) was also analyzed for comparison purposes. The potential of the Pt ring electrode was kept constant at 1.5 V during all measurements to ensure that all the hydroperoxide anion (HO_2^-) reaching the Pt ring was oxidized. Then, the number of electrons transferred (n) was determined as follows:

$$n = \frac{4\, I_{disk}}{I_{disk} + I_{ring}/N}$$

where I_{disk} and I_{ring} are the current measured at the disk and ring electrode, respectively, and N is the collection efficiency of the ring electrode that has been experimentally determined to be 0.37.

Finally, a stability test was performed for CNovel_Fe_2 by chronoamperometric measurements in which the working electrode was kept at 0.65 V in 0.1 M KOH O_2-saturated electrolyte and a rotation rate of 1600 rpm for 3 h. After 3 h, a solution of 1 M CH_3OH was added to the working electrolyte and the data was recorded for an additional 1 h.

3. Results and discussion

3.1. Morphological and physico-chemical characterization

The two commercial carbon supports (Vulcan and CNovel) were ball-milled in the presence of M-phthalocyanines (MPc) under the conditions detailed above. The microstructure and the morphology of the materials were studied by TEM and SEM. Fig. 1 shows TEM images for all the prepared samples. Fig. 1A–D presents the micrographs of the pristine carbon materials before (CNovel and Vulcan) and after grinding (CNovel_m and Vulcan_m). They reveal significant structural differences between the two carbon materials after the ball-milling. On the one hand, unmodified CNovel (Fig. 1A) is made up by hollow shell-like structures of about 100–200 nm of diameter, with walls formed by few carbon layers and with a high external and internal surface. These observations agree with previous results in which CNovel also contains interconnected pores in the three-dimensional network structure [27,28]. After milling, CNovel presents some partial breakage and sintering between spherical structures (Fig. 1B), thus creating additional surface which usually shows higher chemical reactivity [46]. Nevertheless, most of their characteristic structural properties seem to be unaltered. On the other hand, Vulcan (Fig. 1C) is a well-known carbon black composed of spherical aggregates with a diameter of about 30 nm [64] and the milling process does not produce important changes apart from some compaction of these aggregates (Fig. 1D). Comparing both carbon supports, Vulcan apparently has a smaller accessible surface than CNovel. This can significantly affect the correct distribution of the MPc on its surface, which tend to aggregate and stack together [20,65]. Fig. 1E–H and Fig. 1I-L shows the TEM images of CoPc and FePc containing samples after ball-milling, respectively. In both cases, a notable incorporation of defects and an increase in compactness compared to the pristine ball-milled carbon materials are observed, mainly associated with high-energy chemical interactions between the metallic macromolecules and the carbon supports. When the amount of CoPc is 2 wt % (Fig. 1F and H), 1D structures of rectangular shape are clearly appreciated that can be associated to stacked CoPc molecules, as can be seen in Fig. S1A. Some structural changes in the carbon materials induced by the high energy ball-milling cannot be discarded, especially considering that Fe and Co are well-known catalysts for the synthesis of nanostructured carbon materials [66].

Fig. 2 contains the SEM micrographs obtained for CNovel_M_2 and Vulcan_M_2 (M = Co or Fe), as well as the distribution of Co and Fe on both carbon materials as determined by EDX mapping (Co in green and Fe in red). EDX mapping indicates that the MPc are more homogeneously distributed on CNovel (Fig. 2A and B) than on Vulcan (Fig. 2C and D). According to other works in which 3D nanoporous materials were compared with Vulcan, the larger accessible surface of the nanocarbon support allows a more uniform adsorption of MPc as single molecules [21]. In addition, FePc (Fig. 2B and C) seems to present a higher degree of aggregation than CoPc (Fig. 2A and C).

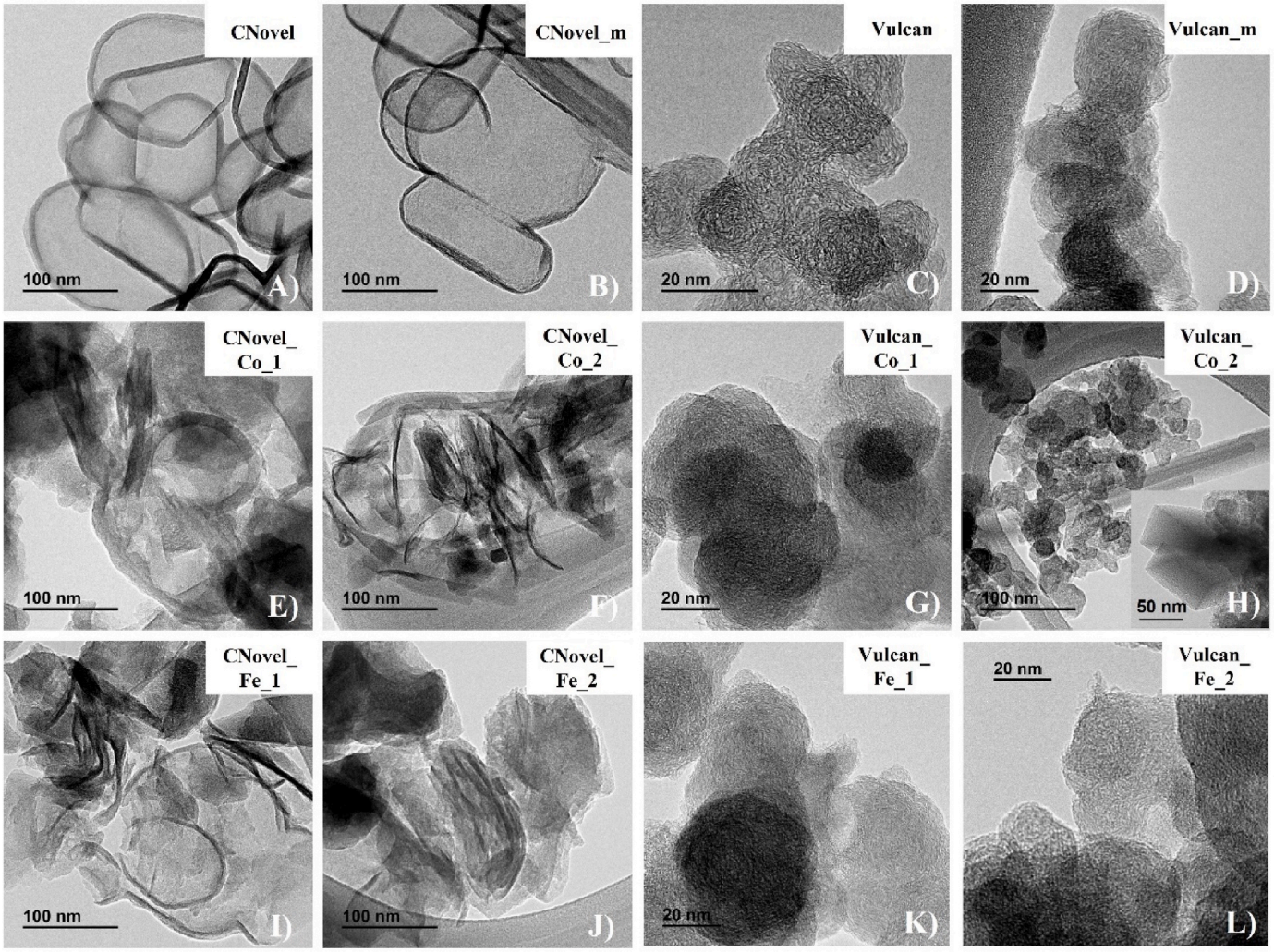

Fig. 1. TEM images of A) CNovel, B) CNovel_m, C) Vulcan, D) Vulcan_m, E) CNovel_Co_1, F) CNovel_Co_2, G) Vulcan_Co_1, H) Vulcan_Co_2, I) CNovel_Fe_1, J) CNovel_Fe_2, K) Vulcan_Fe_1 and L) Vulcan_Fe_2. Inset in H): Magnification of the 1D structures formed during the preparation of Vulcan_Co_2.

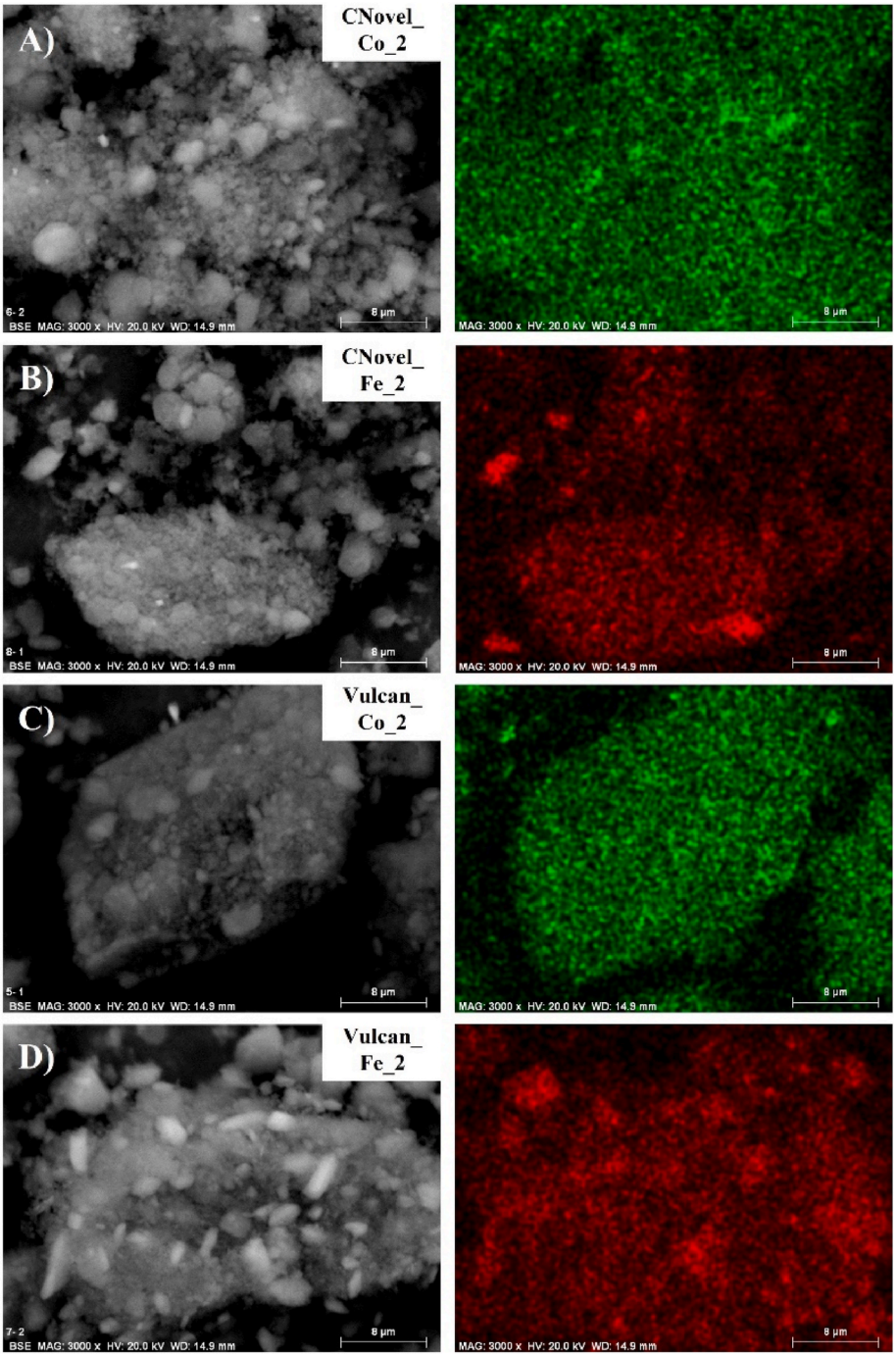

Fig. 2. SEM-EDX micrographs and metal mapping analysis of A) CNovel_Co_2, B) CNovel_Fe_2, C) Vulcan_Co_2 and D) Vulcan_Fe_2. (A colour version of this figure can be viewed online.)

Fig. 3 presents the XRD patterns for the different materials. It should be noted that no relevant changes are appreciated in the diffractograms of the carbon materials before and after milling, being the diffractogram typical of carbon materials with low crystallinity. After the incorporation of MPc, some small peaks are observed in the XRD, especially for the Vulcan support, that are related to the CoPc and FePc species (Fig. S2), since these molecules have a high tendency to aggregate by stacking through the aromatic rings [65]. The XRD patterns are in good agreement with the SEM-EDX observations (Fig. 2) in which a better distribution of MPc occurs for CNovel material probably due to its higher accessible surface. Therefore, these results suggest that CNovel has a more suitable structure and morphology for an adequate distribution and interaction with the MPc.

Porous texture of the materials was analyzed by N_2 adsorption-desorption isotherms. Fig. S3 contains the N_2 adsorption isotherms for the materials and the textural properties obtained are compiled in Table 1, including the BET surface area (S_{BET}) and the micropore volume (V_{DR}). According to the IUPAC classification [67], The N_2 isotherm for CNovel sample is of type IV and for Vulcan it is of type II, in agreement with the morphological observations. The isotherms do not show significant changes after milling (samples CNovel_m and Vulcan_m), although some changes in the hysteresis cycle is observed for CNovel after milling probably due to the breakage of some spherical particles. However, after incorporation of MPc and milling, important changes are

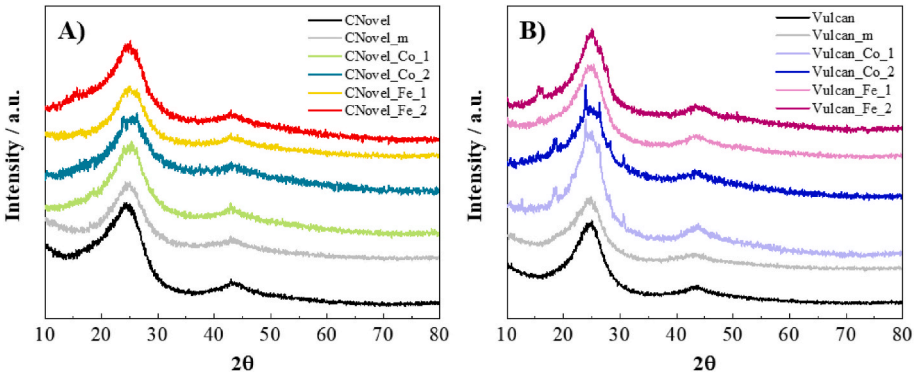

Fig. 3. XRD diffraction patters of A) CNovel and B) Vulcan related samples. (A colour version of this figure can be viewed online.)

Table 1
Porous texture, results of XPS analysis and total metal composition of the different Co- and Fe-related electrocatalysts, as well as the unmodified carbon materials.

Sample	S_{BET}/m^2 g^{-1}	V_{DR}/cm^3 g^{-1}	C_{XPS}/at. %	N_{XPS}/at. %	O_{XPS}/at. %	M_{XPS}/at. % (wt. %)	N/M_{XPS}[a]	M_{ICP}/wt. %
CNovel	258	0.11	95.5	–	4.5	–	–	–
CNovel_m	235	0.10	95.6	–	4.4	–	–	–
CNovel_Co_1	120	0.07	89.1	2.4	8.2	0.4 (1.6)	7	1.1
CNovel_Co_2	75	0.04	87.4	4.2	7.9	0.5 (2.3)	8	1.9
CNovel_Fe_1	125	0.05	90.9	1.1	7.6	0.2 (1.0)	6	0.9
CNovel_Fe_2	89	0.04	88.5	3.8	7.3	0.5 (2.0)	8	2.1
Vulcan	247	0.11	97.0	–	3.0	–	–	–
Vulcan_m	212	0.09	95.6	–	4.4	–	–	–
Vulcan_Co_1	108	0.06	92.9	1.4	5.6	0.2 (0.8)	9	1.0
Vulcan_Co_2	69	0.03	92.4	3.4	3.7	0.5 (2.2)	7	1.9
Vulcan_Fe_1	99	0.05	92.8	0.9	2.1	0.2 (0.7)	6	1.0
Vulcan_Fe_2	63	0.03	91.4	2.4	5.9	0.3 (1.4)	7	2.0

[a] The N atomic content of Vulcan_m obtained by XPS has been subtracted for the calculation of Vulcan-related samples.

observed in the isotherms. Thus, the isotherms of the milled samples in presence of the MPc are nearly parallel to those for the CNovel_m and Vulcan_m samples but they have a very important decrease in the adsorption capacity at low relative pressures. This agrees with the structural changes and material compaction observed by TEM, that occurs when the milling is performed in presence of the MPc and that seems to be promoted by the stacking properties of the MPc.

If we take into account the S_{BET} of CNovel and Vulcan supports (258 and 247 m^2 g^{-1}, respectively), and the area covered by a FePc and CoPc molecule (with an average of 2.17 nm^2 and 2.16 nm^2, respectively, from the optimized molecule using the software *Avogadro*, considering a square geometry and van der Waals radii of the peripheral hydrogen atoms [68]), we can estimate the theoretical MPc:carbon material weight ratio to reach a single monolayer of MPc on the carbon material, being of 0.11 for both CNovel and Vulcan. In this work, the experimental weight ratio is shown in Table S1, with values about 0.11–0.13 (for samples with 1 wt % of metal) and 0.25–0.29 (for samples with 2 wt % of metal), the first one being close to the theoretical value. Therefore, it is expected that MPc in samples with 2 wt % are more stacked and with a worse distribution on the carbon supports, what is in agreement with XRD and TEM results.

The chemical surface composition of the samples was characterized by XPS (Fig. 4 and Table 1). After the ball-milling treatment, similar surface oxygen contents are found for both samples although it is slightly higher for Vulcan_m. In the case of CNovel samples and after milling in presence of MPc, some increase in the oxygen content is observed that can be explained considering that the milling is done in presence of air and that the materials experience important structural changes, with an important breakage of the nanospheres (see Fig. 1). On the contrary, this increase in oxygen content is not observed for Vulcan derived sample in agreement with the structure of pristine Vulcan nanoparticles and the minor structural changes after milling in presence of MPc [54].

Table 1 shows the Co or Fe and N contents which are essentially associated with the macrocycles. It can be observed that the mass percentage (in parentheses in Table 1) is close to the nominal (1 or 2 wt % Co or Fe). In addition, the nitrogen/metal (N/M) ratio is close to the theoretical one (8:1) in MPc molecules, which suggests that the MPc maintain their structure after ball-milling. The metal content determined by ICP-OES is very close to the obtained by XPS (between 0.9 and 1.1 wt % and 1.9–2.1 wt %, respectively) and to the nominal one, which indicates the homogeneous distribution of the MPc on the carbon materials.

N1s, Co2p and Fe2p XPS spectra were analyzed and compared in Fig. 4 to characterize the binding states of these elements in the electrocatalysts. Co2p spectra in Fig. 4A contain a main peak at around 780.6 eV due to $Co2p_{3/2}$ photoelectrons and the corresponding $Co2p_{1/2}$ peak at 796.2 eV, which are characteristic of paramagnetic Co(II) species. In addition, the $Co2p_{3/2}$ contribution is accompanied by a shoulder at around 1.9 eV (782.5 eV) related to the presence of low spin ($S = 1/2$) Co(II) species [69,70]. Moreover, a low-intensity shake-up satellite peak located at 789.9 eV (i.e., 9.3 eV at higher binding energies of the main $Co2p_{3/2}$ peak) indicates the presence of low spin ($S = 0$) diamagnetic Co (III) species but with a minor contribution [69–71]. The last contribution could be a consequence of the stacked structure of CoPc molecules, since this is not noticeable in the supported samples. It is also remarkable that the different features observed for the CoPc, appear in the CoPc-carbon material samples at the same binding energies, and only a slight increase in the asymmetry of the main $Co2p_{3/2}$ peak is appreciable at higher metal loadings. This means that Co–N_4 bonds are essentially unaltered in the Co-based electrocatalysts.

The high resolution XPS spectra of Fe2p (Fig. 4C) for Fe-containing samples show two asymmetric peaks at around 709.3 eV and 722.4 eV belonging to the $Fe2p_{3/2}$ and $Fe2p_{1/2}$ photoelectrons of Fe(II),

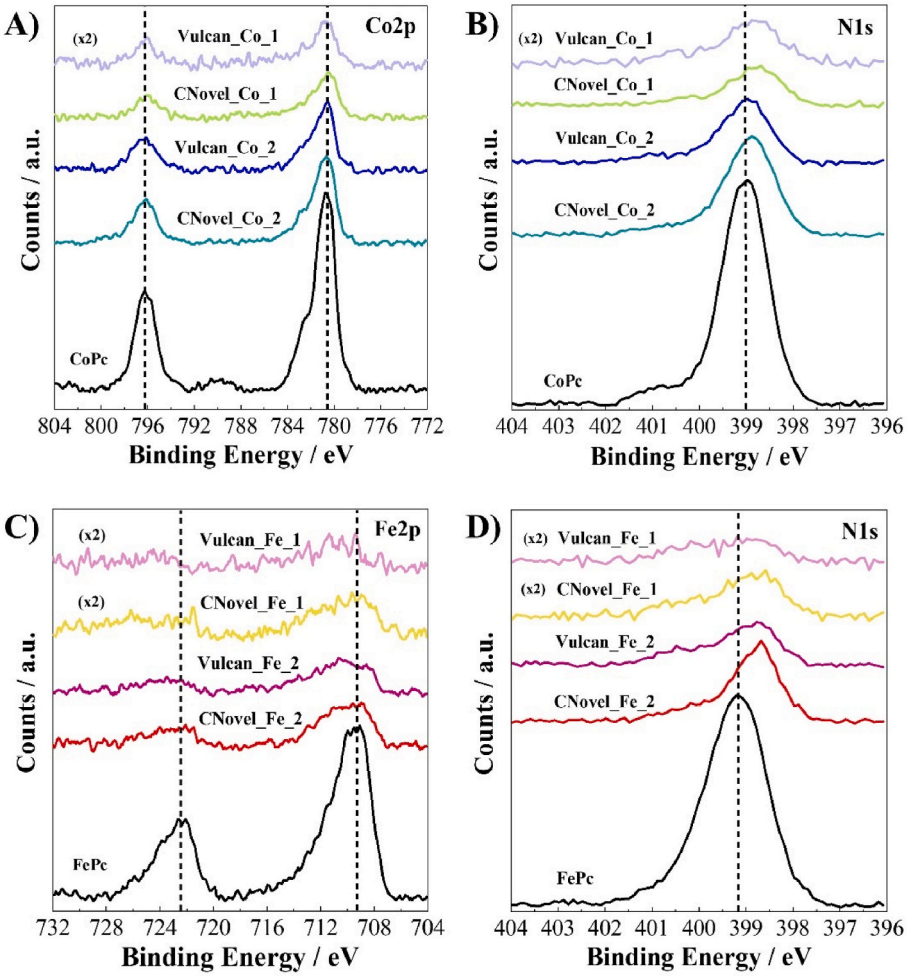

Fig. 4. XPS spectra for A) Co2p and B) N1s of Co-containing samples and C) Fe2p and D) N1s of Fe-containing samples. (A colour version of this figure can be viewed online.)

respectively. The shoulders at higher binding energies can be related to Fe(III) [36]. Interestingly, FePc-containing samples show wider contributions at higher binding energies (~710 eV) than those of pure FePc. This effect could be due to higher interactions of FePc molecules with carbon materials, which affects the chemical surroundings of the Fe–N_4 coordination in FePc and leads to a decrease in the electron density of the Fe atom [36,57,72].

The N1s spectra in Fig. 4B and D shows a major peak at 398.8 eV, which comprises two different N contributions in both MPc molecules with close binding energies [35]. Minor peaks at higher binding energies could be related to impurities in the CoPc and FePc. XPS full survey spectra of FePc and CoPc are shown in Fig. S4, in which no metallic traces residues were detected. Instead, the presence of oxygen (5.1 and 4.9 wt% in FePc and CoPc, respectively) as well as the higher N/Fe or N/Co atomic ratio with respect to the theoretical value of 8 (9.2 and 8.8 in FePc and CoPc, respectively) could be related to impurities from the precursors, such as phthalonitrile, phthalic anhydride, phthalic acid and phthalimide species [73]. A slight shift of N1s peak (~0.5 eV, Fig. 4) can also be observed, especially for FePc-containing materials, probably due to the interaction with the carbon support that generates some electron transfer to the N species in the Fe–N_4 structures.

Fig. 5 shows the TG profiles for the supported metal phthalocyanines and the pristine carbon materials (Fig. 5A and B) and the corresponding CO desorption profiles (Fig. 5C and D). Regarding TG experiments, both carbon supports do not show substantial changes before and after ball-milling. TPD experiments for the carbon materials show higher CO and CO_2 evolution for pristine CNovel and after milling, indicating a higher amount of surface oxygen groups in this material compared to Vulcan. The monitored CO_2 signals are also shown in Fig. S5, which are primarily related to the decomposition of acidic groups. However, the desorbed amount is small and without significant differences in all cases. Table S2 shows the total amounts of CO and CO_2 released during the experiments for each sample. The total oxygen content is estimated from the amount of CO + 2 CO_2 (μmol g^{-1}). Despite similar surface oxygen content in CNovel and Vulcan (slightly higher in CNovel), as obtained from XPS results in Table 1, the total oxygen amount (including the bulk oxygen content), as determined from TPD, is quite different, more than two times higher in CNovel than in Vulcan (Table S2).

The presence of the MPc produces important differences in the TG profiles due to the decomposition of the MPc and further reactions with the carbon material. Taking into account that MPc decomposition starts at around 550 °C [35], the results show that the decomposition of the MPc shifts to higher temperatures in all the cases except for sample Vulcan_Co_2, in which a significant stacking was observed by XRD. This is in agreement with previous results in which a strong interaction between the MPc and the carbon material was observed [35]. This decomposition that occurs at higher temperatures is accompanied by reduction reactions with the carbon materials as deduced from the CO evolution detected in the TPD profile (Fig. 5C and D). In the case of FePc containing materials an additional weight loss is observed in all the cases from 200 to 500 °C that can be associated to some decomposition reactions involving the breakdown of the macrocycles that may occur in this compound [74,75].

It is worth noting that the presence of FePc molecules produces an

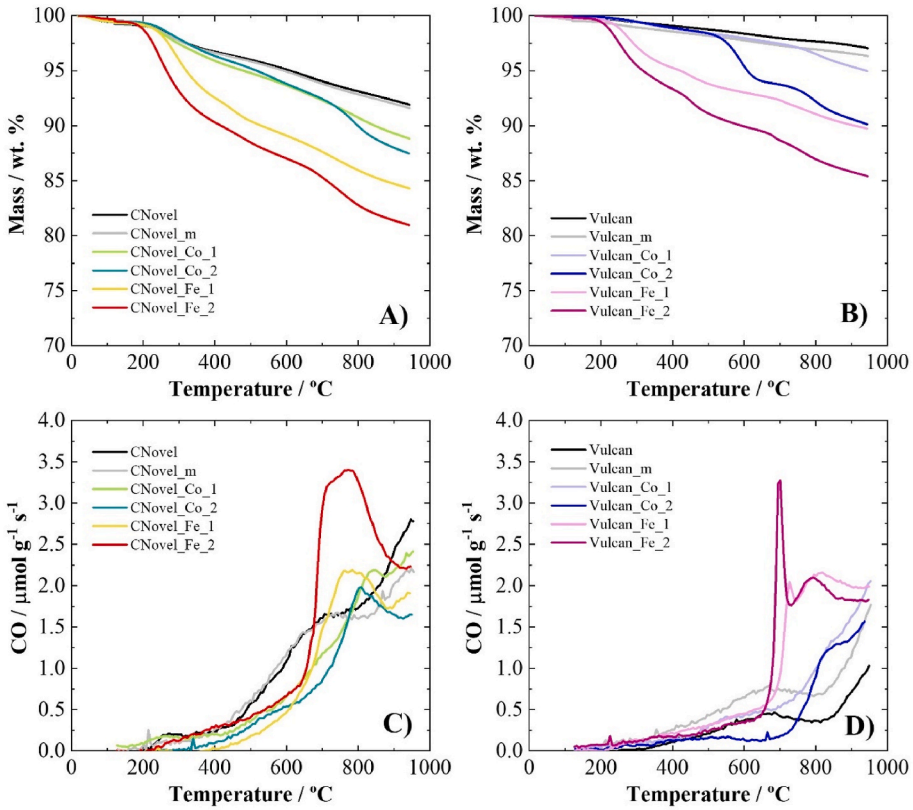

Fig. 5. Weight loss during the thermogravimetric analysis of CoPc and FePc supported on A) CNovel and B) Vulcan, as well as for the pristine carbon samples. CO desorption profiles for C) CNovel and D) Vulcan-related samples performed in He atmosphere at heating rate of 20 °C min^{-1}. (A colour version of this figure can be viewed online.)

additional CO peak at 700 °C in comparison with CoPc-related materials, indicating slightly different decomposition pathways for FePc and CoPc [37]. Moreover, the last peak is more well-defined when they are combined with Vulcan than with CNovel support, where more homogeneous or heterogeneous species intervene, respectively. This observation is in agreement with the better distribution observed by TEM (Fig. 1) for the MPc on the CNovel support. In addition, differences in oxygen content after MPc incorporation, both on the surface and at the bulk, are observed in Table 1 and Table S2 compared to non-modified carbon materials, could be related to structural changes during milling treatment, as previously suggested, which are more evident for CNovel than for Vulcan related samples. Therefore, these results clearly confirm the influence of the metal center in MPc and the carbon support on the thermal decomposition mechanisms.

3.2. Electrochemical characterization

Fig. 6A and B contain the steady state cyclic voltammograms (CVs) of all prepared catalysts in N_2-saturated atmosphere and 0.1 M KOH solution. Within the potential window studied, CVs of CNovel_m and Vulcan_m show the typical shape characteristic of carbon materials due to the electrical double-layer charging processes.

When MPc molecules are incorporated, CVs present redox processes characteristic of the MPc. Then, CoPc-containing samples show a redox process at around 0.37 V attributed to the Co(I)/Co(II) reaction and the Co(II)/Co(III) redox peak does not appear in this potential range [76, 77]. FePc-containing samples present two redox transitions at approximately 0.35 V and 0.80 V, corresponding to the Fe(I)/Fe(II) and Fe (II)/Fe(III) redox couples, respectively [78]. These redox processes are more intense for samples with a higher loading of FePc.

Table S3 shows the peak potentials for Co(I)/Co(II) and Fe(II)/Fe(III) redox couple observed in the voltammograms for the different electrocatalysts. In general, the use of CNovel slightly shifts the peak potential to higher values, which could be beneficial for the ORR. According to other authors [36], it is possible that the higher oxygen content in CNovel than in Vulcan modified samples (as observed in the TPD experiments) could lead to interactions with MPc molecules promoting axial coordination with the metal central atom that imply an electron-pulling effect and a favorable electronic distribution.

Fig. 6C and D displays the CVs in O_2-saturated 0.1 M KOH electrolyte for the catalysts with the best catalytic response. The other CVs are found in Fig. S6. The electrochemical reduction of oxygen is detected as an increase in current (in absolute value) in the cathodic scan, which appears at higher potential values (lower overpotential) for all FePc-containing samples, as expected, especially when CNovel is used as support.

3.2.1. Study of the electrocatalytic activity towards ORR

The electrocatalytic activity of the prepared electrocatalysts towards ORR was studied using a rotating ring-disk electrode (RRDE) in O_2-saturated 0.1 M KOH electrolyte. Fig. 7 shows both linear sweep voltammetry (LSV) curves and the number of electrons transferred (n) during the ORR obtained for all electrocatalysts, as well as for the commercial Pt/C (20 wt % Pt), at 1600 rpm and 5 mV s^{-1} from 1.0 V to 0.0 V. In addition, Table 2 summarizes the most relevant kinetic parameters derived from RRDE experiments during the electrochemical reduction of O_2. It should be mentioned that, in this work, the onset potential is defined at a current density of −0.1 mA cm^{-2} in the LSV curves, the n values are measured at 0.7 V and the limiting current density (j_{lim}) is set at 0.4 V.

As seen in Fig. 7A and B, a notable improvement in the electrocatalytic performance occurs for all the MPc-containing samples in terms of the onset potential with respect to the unmodified carbon materials (CNovel_m and Vulcan_m). However, only CNovel_Fe_2 shows

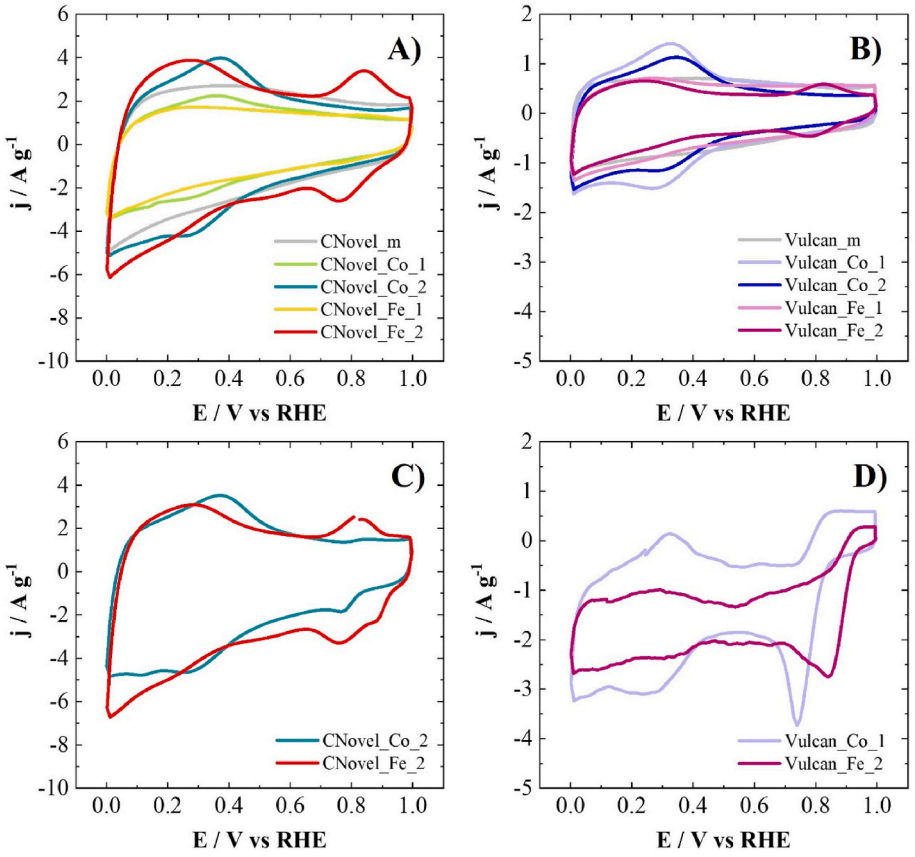

Fig. 6. Cyclic voltammograms in N_2-saturated for A) CNovel-related catalysts and B) Vulcan-related catalysts. Cyclic voltammograms in O_2-saturated for C) CNovel_Co_2 and CNovel_Fe_2 catalysts and D) Vulcan_Co_1 and Vulcan_Fe_2 catalysts. 0.1 M KOH electrolyte at 50 mV s^{-1}. (A colour version of this figure can be viewed online.)

a completely flat limiting current in the LSV curve and its performance is the closest to the commercial Pt-containing catalyst. These results confirm that MPc play an important role in the electrocatalysis of the ORR. Nonetheless, as it is well-known from the literature [12], the ORR performance and redox mechanism are highly influenced by the nature of the metal in the MPc molecules and by the synergistic effect between these macrocycles and the carbon support. In this sense, FePc-containing catalysts show a better ORR response than those modified with CoPc, which could be explained through different activity descriptors such as the M(III)/M(II) redox potential, the number of d electrons of the transition metal (d^6 for Fe(II) and d^7 for Co(II)) and the donor-acceptor intermolecular interaction of N_4-*M*-O_2 or their intermediates, among others [12]. Previous studies have shown that the activity of FePc supported on carbon nanotubes, graphene or carbon black is related to the adsorption of the dioxygen molecule in the vicinity of Fe, which weakens the *O*–O bond as an essential requirement for the ORR to follow the desired 4-electron route [79]. Fig. 7C and D confirm the mentioned 4-electron pathway for all FePc-containing samples, following the same trend as Pt/C catalyst. Therefore, low amounts of HO_2^- are produced and monitored by the Pt ring electrode (Fig. S7), which can be beneficial to avoid the oxidation of MPc that would result in a poor electrochemical durability, together with the demetallation [80].

Different electrochemical behavior is observed in the selectivity of CoPc supported on both carbon materials, where *n* between 2.5 and 3 suggests a combination of a 4 and 2-electron mechanism or 2 + 2 electron pathway, different from the typical 2-electron mechanism reported in the literature for Co-containing samples [79], but similar to what has recently been described for CoN_5 species [76] due to stronger O_2 bonding energy. Therefore, just by changing the metal ion in the phthalocyanines and the carbon support, different products could be obtained and Co-related catalysts could be used for the H_2O_2/HO_2^- production [81].

Comparing both carbon supports, it seems that CNovel, with the presence of hollow-nanospheres that may act as efficient nanoreactors, shows a more adequate structure than Vulcan for the correct distribution and interaction with MPc molecules that promotes a more favorable environment for an enhanced ORR under the studied conditions. Previous studies [29] demonstrated the better electrocatalytic performance of this porous material (CNovel) compared to Vulcan for loading Pt nanoparticles, which was also attributed to the lower ionomer coverage of metal sites. Additionally, Fig. S8 shows the LSV curves of CNovel_Fe_2 and CNovel_Co_2 prepared in different batches, which suggest an acceptable reproducibility of the catalysts prepared by the one-step ball-milling method in ambient conditions.

3.2.2. *Stability analysis of FePc-containing catalysts towards ORR*

Long-term durability is one of the major challenges when using MPc molecules as electrocatalysts in fuel cell technology [80]. The stability of the CNovel_Fe_2 catalyst was evaluated under potentiostatic conditions, since it was the catalyst with the best performance towards ORR. Fig. 8 shows the normalized current versus time recorded at 0.65 V in 0.1 M KOH O_2-saturated atmosphere and at 1600 rpm for CNovel_Fe_2 and Pt/C for comparative purposes. After 3 h, an additional hour was recorded in the presence of 1 M CH_3OH solution to study the possible use in direct methanol fuel cells. Interestingly, CNovel_Fe_2 shows the same trend as Pt/C during the first 3 h, where the current remains almost constant at 97% of the initial value. When methanol was added, only a small loss of 5% appears in CNovel_Fe_2, while Pt/C is affected by a huge decrease in ORR activity due to poisoning effect. Therefore, these results indicate the excellent stability of the prepared electrocatalyst in alkaline

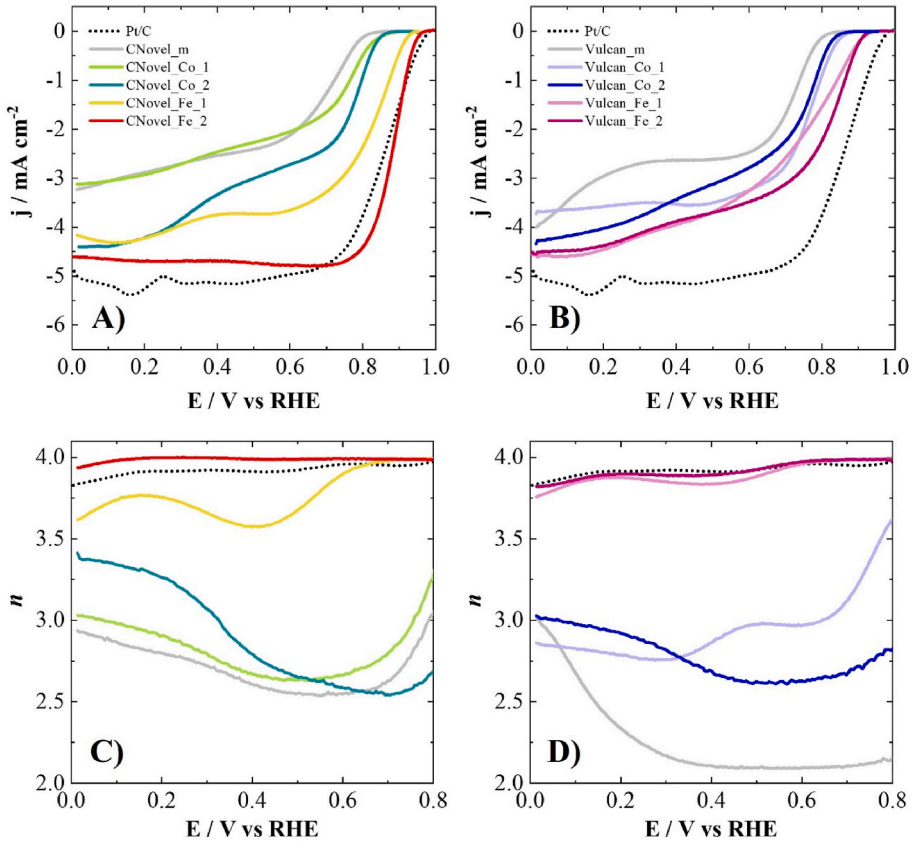

Fig. 7. LSV curves and number of electrons transferred (*n*) per oxygen molecule for ORR, for A, C) CNovel-related electrocatalysts and B, D) Vulcan-related electrocatalysts and Pt/C, in O_2-saturated 0.1 M KOH solution at 1600 rpm and 5 mV s^{-1}. (A colour version of this figure can be viewed online.)

Table 2
Electrochemical data of CNovel, Vulcan and each respective electrocatalysts with CoPc and FePc molecules at different metal loading, together with comparison with Pt/C in O_2-saturated 0.1 M KOH solution.

Sample	E_{ONSET}[a]/V vs RHE	n[b]	j_{lim}[c]/mA cm^{-2}
20 wt % Pt/C	0.97	3.95	−5.14
CNovel_m	0.81	2.63	−2.54
CNovel_Co_1	0.85	2.80	−2.46
CNovel_Co_2	0.85	2.54	−3.34
CNovel_Fe_1	0.93	3.98	−3.74
CNovel_Fe_2	0.95	3.99	−4.69
Vulcan_m	0.81	2.10	−2.63
Vulcan_Co_1	0.86	3.12	−3.53
Vulcan_Co_2	0.84	2.68	−3.42
Vulcan_Fe_1	0.92	3.98	−3.95
Vulcan_Fe_2	0.92	3.99	−3.88

[a] Determined at −0.1 mA cm^{-2}.
[b] Determined at 0.7 V vs RHE.
[c] Determined at 0.4 V vs RHE.

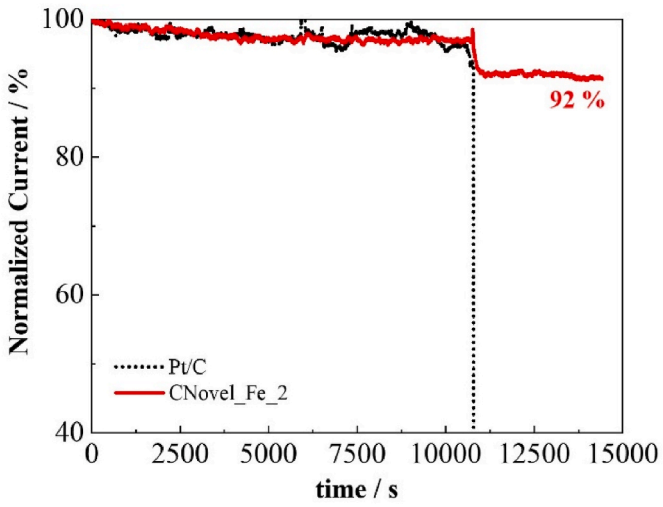

Fig. 8. Chronoamperometric curves of CNovel_Fe_2 and Pt/C electrode at 0.65 V in O_2-saturated 0.1 M KOH electrolyte. 1600 rpm (T = 25 °C). (A colour version of this figure can be viewed online.)

medium. Acidic conditions were also explored for CNovel_Fe_2, which was also active for ORR at low pH, but stability should be improved (see Fig. S9). Further studies will be focused on optimizing ball-milling conditions to extend one-step mechanochemical synthesis of efficient catalysts for ORR over a wide range of pH.

4. Conclusions

Different electrocatalysts for the ORR based on cobalt(II) and iron(II) phthalocyanines supported on commercial carbon materials (CNovel and Vulcan) have been prepared by a solid-state ball-milling method in ambient and dry conditions, which allows to grind large quantities of materials in a relatively short time with high yields and without causing significant damage to the structure of the carbon materials. Two carbon materials with different structures have been used, CNovel and Vulcan. CNovel is constituted by spherical hollow nanospheres that provide both high external and internal surface where MPc can be incorporated and homogeneously distributed. Vulcan carbon black is made up of spherical nanoparticles with some degree of aggregation with a smaller surface

area where MPc are more likely to aggregate and stack together, what is clearly observed for FePc.

The electrocatalytic activity of the materials obtained for the ORR in alkaline medium, show that the best performance corresponds to FePc when supported on CNovel carbon material, what is in agreement with the better distribution of MPc due to its hollow-like spherical structure. Although some FePc stacking and material compaction can occur when using 2 wt % of metal loading, CNovel seems to promote a better interaction and a more homogeneous distribution than in Vulcan under the same conditions. This effect could be connected not only to the more accessible surface, but also to the presence of higher oxygen content in CNovel (as seen in the TPD experiments) that can coordinate with the central metal in FePc and promote favorable electronic redistribution for ORR electrocatalysis. These results are supported by changes in XPS spectra for FePc-related samples, whereas for CoPc-related catalysts they are practically unaltered. Consistent with these findings, CNovel_Fe_2 sample provides excellent electrocatalytic properties, in terms of electrocatalytic activity, long-term stability and methanol tolerance compared to a commercial Pt/C catalyst, which are even more remarkable for its ease of preparation.

Direct contact between MPc and the carbon support using a ball-milling method and under dry conditions, that is without the use of any solvent, produces electrocatalysts with excellent performance. As a main achievement of this study, this work provides important insights on one-step solvent-free mechanochemical preparation method of efficient molecular electrocatalysts for ORR, in which no pre-treatment (e.g., functionalization of the carbon support), solvent addition or post-processing steps (e.g., heat-treatment, acid-treatment, etc.) were required before, during or after the ball-milling procedure.

CRediT authorship contribution statement

Alicia Trigueros-Sancho: Authors contributed equally to this work. **Beatriz Martínez-Sánchez:** Authors contributed equally to this work. **Diego Cazorla-Amorós:** Authors contributed equally to this work. **Emilia Morallón:** Authors contributed equally to this work.

Declaration of competing interest

The authors declare that they have no known competing financial interests or personal relationships that could have appeared to influence the work reported in this paper.

Acknowledgments

B.M.-S. thanks “Ministerio de Universidades” for the FPU grant (FPU18/05127). The authors would like to thank PID2019-105923RB-I00 and PID2021-123079OB-I00 projects funded by MCIN/AEI/10.13039/501100011033 and “ERDF A way of making Europe”.

Appendix A. Supplementary data

Supplementary data to this article can be found online at https://doi.org/10.1016/j.carbon.2023.118100.

References

[1] M.K. Debe, Electrocatalyst approaches and challenges for automotive fuel cells, Nature 486 (2012) 43–51, https://doi.org/10.1038/nature11115.
[2] Y. Wang, K.S. Chen, J. Mishler, S.C. Cho, X.C. Adroher, A review of polymer electrolyte membrane fuel cells: technology, applications, and needs on fundamental research, Appl. Energy 88 (2011) 981–1007, https://doi.org/10.1016/j.apenergy.2010.09.030.
[3] R. Cao, J.-S. Lee, M. Liu, J. Cho, Recent progress in non-precious catalysts for metal-air batteries, Adv. Energy Mater. 2 (2012) 816–829, https://doi.org/10.1002/aenm.201200013.
[4] X. Yu, S. Ye, Recent advances in activity and durability enhancement of Pt/C catalytic cathode in PEMFC, J. Power Sources 172 (2007) 133–144, https://doi.org/10.1016/j.jpowsour.2007.07.049.
[5] F.S. Saleh, E.B. Easton, Assessment of the ethanol oxidation activity and durability of Pt catalysts with or without a carbon support using Electrochemical Impedance Spectroscopy, J. Power Sources 246 (2014) 392–401, https://doi.org/10.1016/j.jpowsour.2013.07.109.
[6] Z. Liang, H. Zheng, R. Cao, Importance of electrocatalyst morphology for the oxygen reduction reaction, Chemelectrochem 6 (2019) 2600–2614, https://doi.org/10.1002/celc.201801859.
[7] Y. Liu, X. Yue, K. Li, J. Qiao, D.P. Wilkinson, J. Zhang, PEM fuel cell electrocatalysts based on transition metal macrocyclic compounds, Coord. Chem. Rev. 315 (2016) 153–177, https://doi.org/10.1016/j.ccr.2016.02.002.
[8] Y. Jiao, Y. Zheng, M. Jaroniec, S.Z. Qiao, Design of electrocatalysts for oxygen- and hydrogen-involving energy conversion reactions, Chem. Soc. Rev. 44 (2015) 2060–2086, https://doi.org/10.1039/C4CS00470A.
[9] K. Singh, F. Razmjooei, J.-S. Yu, Active sites and factors influencing them for efficient oxygen reduction reaction in metal-N coordinated pyrolyzed and non-pyrolyzed catalysts: a review, J. Mater. Chem. 5 (2017) 20095–20119, https://doi.org/10.1039/C7TA05222G.
[10] R. Jasinski, A new fuel cell cathode catalyst, Nature 201 (1964) 1212–1213, https://doi.org/10.1038/2011212a0.
[11] A. Kumar, S. Ibraheem, T. Anh Nguyen, R.K. Gupta, T. Maiyalagan, G. Yasin, Molecular-MN4 vs atomically dispersed M−N_4−C electrocatalysts for oxygen reduction reaction, Coord. Chem. Rev. 446 (2021), 214122, https://doi.org/10.1016/j.ccr.2021.214122.
[12] J.H. Zagal, M.T.M. Koper, Reactivity descriptors for the activity of molecular MN_4 catalysts for the oxygen reduction reaction, Angew. Chem. 128 (2016) 14726–14738, https://doi.org/10.1002/ange.201604311.
[13] J.S. Park, D.W. Chang, Iron phthalocyanine/graphene composites as promising electrocatalysts for the oxygen reduction reaction, Energies 13 (2020) 4073, https://doi.org/10.3390/en13164073.
[14] A.B. Sorokin, Phthalocyanine metal complexes in catalysis, Chem. Rev. 113 (2013) 8152–8191, https://doi.org/10.1021/cr4000072.
[15] S. Meshitsuka, M. Ichikawa, K. Tamaru, Electrocatalysis by metal phthalocyanines in the reduction of carbon dioxide, J. Chem. Soc., Chem. Commun. (1974) 158–159, https://doi.org/10.1039/c39740000158.
[16] C.M. Lieber, N.S. Lewis, Catalytic reduction of carbon dioxide at carbon electrodes modified with cobalt phthalocyanine, J. Am. Chem. Soc. 106 (1984) 5033–5034, https://doi.org/10.1021/ja00329a082.
[17] M. Dieng, O. Contamin, M. Savy, Problem of water electrolysis: interest of catalysts containing molybdenum naphthalocyanines, Electrochim. Acta 33 (1988) 121–126, https://doi.org/10.1016/0013-4686(88)80043-4.
[18] N. Chebotareva, T. Nyokong, First-row transition metal phthalocyanines as catalysts for water electrolysis: a comparative study, Electrochim. Acta 42 (1997) 3519–3524, https://doi.org/10.1016/S0013-4686(97)00033-9.
[19] D.D. Eley, Phthalocyanines as semiconductors, Nature 162 (1948) 819, https://doi.org/10.1038/162819a0.
[20] A. Abbaspour, E. Mirahmadi, Electrocatalytic activity of iron and nickel phthalocyanines supported on multi-walled carbon nanotubes towards oxygen evolution reaction, Electrochim. Acta 105 (2013) 92–98, https://doi.org/10.1016/j.electacta.2013.04.143.
[21] J. Yang, J. Tao, T. Isomura, H. Yanagi, I. Moriguchi, N. Nakashima, A comparative study of iron phthalocyanine electrocatalysts supported on different nanocarbons for oxygen reduction reaction, Carbon 145 (2019) 565–571, https://doi.org/10.1016/j.carbon.2019.01.022.
[22] W. Li, C. Liang, J. Qiu, W. Zhou, H. Han, Z. Wei, G. Sun, Q. Xin, Carbon nanotubes as support for cathode catalyst of a direct methanol fuel cell, Carbon 40 (2002) 791–794, https://doi.org/10.1016/S0008-6223(02)00039-8.
[23] Y. Yuan, J. Ahmed, S. Kim, Polyaniline/carbon black composite-supported iron phthalocyanine as an oxygen reduction catalyst for microbial fuel cells, J. Power Sources 196 (2011) 1103–1106, https://doi.org/10.1016/j.jpowsour.2010.08.112.
[24] S. Yang, Y. Yu, X. Gao, Z. Zhang, F. Wang, Recent advances in electrocatalysis with phthalocyanines, Chem. Soc. Rev. 50 (2021) 12985–13011, https://doi.org/10.1039/D0CS01605E.
[25] A. Walcarius, Mesoporous materials and electrochemistry, Chem. Soc. Rev. 42 (2013) 4098–4140, https://doi.org/10.1039/c2cs35322a.
[26] C. Alegre, D. Sebastián, E. Baquedano, M.E. Gálvez, R. Moliner, M. Lázaro, Tailoring synthesis conditions of carbon xerogels towards their utilization as Pt-catalyst supports for oxygen reduction reaction (ORR), Catalysts 2 (2012) 466–489, https://doi.org/10.3390/catal2040466.
[27] A. Sakuda, Y. Sato, A. Hayashi, M. Tatsumisago, Sulfur-based composite electrode with interconnected mesoporous carbon for all-solid-state lithium–sulfur batteries, Energy Technol. 7 (2019), 1900077, https://doi.org/10.1002/ente.201900077.
[28] J. Toyo, Tanso Co. Ltd, (osaka, carbon-graphite products CNovel TM porous carbon). https://www.toyotanso.com/Products/cnovel/. (Accessed 7 January 2022) (n.d.).
[29] Y. Kamitaka, T. Takeshita, Y. Morimoto, MgO-templated mesoporous carbon as a catalyst support for polymer electrolyte fuel cells, Catalysts 8 (2018) 230, https://doi.org/10.3390/catal8060230.
[30] H. Daimon, T. Miyata, S. Yoshikawa, S. Nishikawa, S. Ichikawa, Y. Kishimoto, T. Doi, M. Inaba, Improvements in oxygen diffusivity, ORR activity and durability of Pt-based catalysts by mesoporous carbon support and melamine decoration, ECS Meet. Abstr. MA2022–02 (2022) 1551, https://doi.org/10.1149/MA2022-02421551mtgabs.

[31] S. Nishikawa, T. Miyata, Y. Kishimoto, H. Inoue, H. Daimon, T. Doi, M. Inaba, Improvements in ORR activity and cell performance of Pt-based catalysts for PEFCs by modification with protonated melamine-derivative salts, ECS Meet. Abstr. MA2022–02 (2022) 1561, https://doi.org/10.1149/MA2022-02421561mtgabs.

[32] H. Shintani, N. Miyata, Y. Sugawara, A model for mesoporous carbon-supported platinum catalyst/electrolyte interfaces in polymer electrolyte fuel cells, J. Power Sources 487 (2021), 229414, https://doi.org/10.1016/j.jpowsour.2020.229414.

[33] J. Wang, H. Kong, J. Zhang, Y. Hao, Z. Shao, F. Ciucci, Carbon-based electrocatalysts for sustainable energy applications, Prog. Mater. Sci. 116 (2021), 100717, https://doi.org/10.1016/j.pmatsci.2020.100717.

[34] J.X. Flores-Lasluisa, D. Salinas-Torres, M.V. López-Ramón, M.A. Álvarez, C. Moreno-Castilla, D. Cazorla-Amorós, E. Morallón, Copper ferrite nanospheres composites mixed with carbon black to boost the oxygen reduction reaction, Colloids Surf. A Physicochem. Eng. Asp. 613 (2021), 126060, https://doi.org/10.1016/j.colsurfa.2020.126060.

[35] C. González-Gaitán, R. Ruiz-Rosas, E. Morallón, D. Cazorla-Amorós, Relevance of the interaction between the M-phthalocyanines and carbon nanotubes in the electroactivity toward ORR, Langmuir 33 (2017) 11945–11955, https://doi.org/10.1021/acs.langmuir.7b02579.

[36] X. Yan, X. Xu, Z. Zhong, J. Liu, X. Tian, L. Kang, J. Yao, The effect of oxygen content of carbon nanotubes on the catalytic activity of carbon-based iron phthalocyanine for oxygen reduction reaction, Electrochim. Acta 281 (2018) 562–570, https://doi.org/10.1016/j.electacta.2018.05.183.

[37] V. Bambagioni, C. Bianchini, J. Filippi, A. Lavacchi, W. Oberhauser, A. Marchionni, S. Moneti, F. Vizza, R. Psaro, V. Dal Santo, A. Gallo, S. Recchia, L. Sordelli, Single-site and nanosized Fe–Co electrocatalysts for oxygen reduction: synthesis, characterization and catalytic performance, J. Power Sources 196 (2011) 2519–2529, https://doi.org/10.1016/j.jpowsour.2010.11.030.

[38] J. Quílez-Bermejo, C. González-Gaitán, E. Morallón, D. Cazorla-Amorós, Effect of carbonization conditions of polyaniline on its catalytic activity towards ORR. Some insights about the nature of the active sites, Carbon 119 (2017) 62–71, https://doi.org/10.1016/j.carbon.2017.04.015.

[39] J.H. Zagal, I. Ponce, D. Baez, R. Venegas, J. Pavez, M. Paez, M. Gulppi, A possible interpretation for the high catalytic activity of heat-treated non-precious metal n_x/C catalysts for O_2 reduction in terms of their formal potentials, Electrochem. Solid State Lett. 15 (2012) B90, https://doi.org/10.1149/2.032206esl.

[40] A. Kumar, Y. Zhang, Y. Jia, W. Liu, X. Sun, Redox chemistry of N_4-Fe^{2+} in iron phthalocyanines for oxygen reduction reaction, Chin. J. Catal. 42 (2021) 1404–1412, https://doi.org/10.1016/S1872-2067(20)63731-7.

[41] K.D. Beard, J.W. Van Zee, J.R. Monnier, Preparation of carbon-supported Pt–Pd electrocatalysts with improved physical properties using electroless deposition methods, Appl. Catal., B 88 (2009) 185–193, https://doi.org/10.1016/j.apcatb.2008.09.033.

[42] A. Friedman, L. Landau, S. Gonen, Z. Gross, L. Elbaz, Efficient bio-inspired oxygen reduction electrocatalysis with electropolymerized cobalt corroles, ACS Catal. 8 (2018) 5024–5031, https://doi.org/10.1021/acscatal.8b00876.

[43] S. Domínguez-Domínguez, J. Arias-Pardilla, Á. Berenguer-Murcia, E. Morallón, D. Cazorla-Amorós, Electrochemical deposition of platinum nanoparticles on different carbon supports and conducting polymers, J. Appl. Electrochem. 38 (2008) 259–268, https://doi.org/10.1007/s10800-007-9435-9.

[44] H. Abe, Y. Hirai, S. Ikeda, Y. Matsuo, H. Matsuyama, J. Nakamura, T. Matsue, H. Yabu, Fe azaphthalocyanine unimolecular layers (Fe AzULs) on carbon nanotubes for realizing highly active oxygen reduction reaction (ORR) catalytic electrodes, NPG Asia Mater. 11 (2019) 57, https://doi.org/10.1038/s41427-019-0154-6.

[45] T. Yoshii, K. Chida, H. Nishihara, F. Tani, Ordered carbonaceous frameworks: a new class of carbon materials with molecular-level design, Chem. Commun. 58 (2022) 3578–3590, https://doi.org/10.1039/D1CC07228E.

[46] T. Xing, J. Sunarso, W. Yang, Y. Yin, A.M. Glushenkov, L.H. Li, P.C. Howlett, Y. Chen, Ball milling: a green mechanochemical approach for synthesis of nitrogen doped carbon nanoparticles, Nanoscale 5 (2013) 7970–7976, https://doi.org/10.1039/c3nr02328a.

[47] S.L. James, C.J. Adams, C. Bolm, D. Braga, P. Collier, T. Friščić, F. Grepioni, K.D. M. Harris, G. Hyett, W. Jones, A. Krebs, J. Mack, L. Maini, A.G. Orpen, I.P. Parkin, W.C. Shearouse, J.W. Steed, D.C. Waddell, Mechanochemistry: opportunities for new and cleaner synthesis, Chem. Soc. Rev. 41 (2012) 413–447, https://doi.org/10.1039/C1CS15171A.

[48] H. Wang, W. Wang, Y.Y. Xu, M. Asif, H. Liu, B.Y. Xia, Ball-milling synthesis of Co_2P nanoparticles encapsulated in nitrogen doped hollow carbon rods as efficient electrocatalysts, J. Mater. Chem. A Mater. 5 (2017) 17563–17569, https://doi.org/10.1039/C7TA05510B.

[49] J. Zhu, S. Mu, Defect engineering in carbon-based electrocatalysts: insight into intrinsic carbon defects, Adv. Funct. Mater. 30 (2020), 2001097, https://doi.org/10.1002/adfm.202001097.

[50] C. Gao, Z. Zhao, X. Qin, J. Teng, J. Fan, P. Shi, Q. Xu, Y. Min, Metal-free red phosphorus-black phosphorus/carbon nanotubes heterostructured electrocatalyst for efficient oxygen evolution reaction, Compos. Commun. 24 (2021), 100624, https://doi.org/10.1016/j.coco.2020.100624.

[51] Y. Wang, N. Xu, R. He, L. Peng, D. Cai, J. Qiao, Large-scale defect-engineering tailored tri-doped graphene as a metal-free bifunctional catalyst for superior electrocatalytic oxygen reaction in rechargeable Zn-air battery, Appl. Catal., B 285 (2021), 119811, https://doi.org/10.1016/j.apcatb.2020.119811.

[52] S. Zhang, H. Zhang, X. Hua, S. Chen, Tailoring molecular architectures of Fe phthalocyanine on nanocarbon supports for high oxygen reduction performance, J. Mater. Chem. A Mater. 3 (2015) 10013–10019, https://doi.org/10.1039/C5TA01400J.

[53] C. Karuppiah, B. Thirumalraj, S. Alagar, S. Piraman, Y.-J.J. Li, C.-C. Yang, Solid-state ball-milling of Co_3O_4 nano/microspheres and carbon black endorsed $LaMnO_3$ perovskite catalyst for bifunctional oxygen electrocatalysis, Catalysts 11 (2021) 76, https://doi.org/10.3390/catal11010076.

[54] M.A. Costa de Oliveira, P.P. Machado Pico, W. da Silva Freitas, A. D'Epifanio, B. Mecheri, Iron-based electrocatalysts for energy conversion: effect of ball milling on oxygen reduction activity, Appl. Sci. 10 (2020) 5278, https://doi.org/10.3390/app10155278.

[55] Y. Wang, M. Liu, Y. Zhang, Q. Yi, R. Yi, All-solid-state synthesis of high-performance electrocatalysts for oxygen reduction reaction derived from g-C_3N_4 and cobalt phthalocyanine, Adv. Mater. Interfac. 9 (2022), 2201330, https://doi.org/10.1002/admi.202201330.

[56] T. Liu, F. Sun, M. Huang, L. Guan, Atomically dispersed Co–N–C electrocatalysts synthesized by a low-speed ball milling method for proton exchange membrane fuel cells, Mater.Adv. 3 (2022) 1565–1573, https://doi.org/10.1039/D1MA00809A.

[57] B. Martínez-Sánchez, D. Cazorla-Amorós, E. Morallón, P-functionalized carbon nanotubes promote highly stable electrocatalysts based on Fe-phthalocyanines for oxygen reduction: experimental and computational studies, J. Energy Chem. 72 (2022) 276–290, https://doi.org/10.1016/j.jechem.2022.05.024.

[58] M. Lefèvre, E. Proietti, F. Jaouen, J.-P. Dodelet, Iron-based catalysts with improved oxygen reduction activity in polymer electrolyte fuel cells, Science 324 (2009) 71–74, https://doi.org/10.1126/science.1170051 (1979).

[59] H. Meng, F. Jaouen, E. Proietti, M. Lefèvre, J.P. Dodelet, pH-effect on oxygen reduction activity of Fe-based electro-catalysts, Electrochem. Commun. 11 (2009) 1986–1989, https://doi.org/10.1016/j.elecom.2009.08.035.

[60] E. Proietti, F. Jaouen, M. Lefèvre, N. Larouche, J. Tian, J. Herranz, J.P. Dodelet, Iron-based cathode catalyst with enhanced power density in polymer electrolyte membrane fuel cells, Nat. Commun. 2 (2011), https://doi.org/10.1038/ncomms1427.

[61] F. Jaouen, V. Goellner, M. Lefèvre, J. Herranz, E. Proietti, J.P. Dodelet, Oxygen reduction activities compared in rotating-disk electrode and proton exchange membrane fuel cells for highly active FeNC catalysts, Electrochim. Acta 87 (2013) 619–628, https://doi.org/10.1016/j.electacta.2012.09.057.

[62] X. Tan, H. Li, W. Zhang, K. Jiang, S. Zhai, W. Zhang, N. Chen, H. Li, Z. Li, Square-pyramidal Fe-N_4 with defect-modulated O-coordination: two-tier electronic structure fine-tuning for enhanced oxygen reduction, Chem Catal. 2 (2022) 816–835, https://doi.org/10.1016/j.checat.2022.01.025.

[63] S. Brunauer, P.H. Emmett, E. Teller, Adsorption of gases in multimolecular layers, J. Am. Chem. Soc. 60 (1938) 309–319, https://doi.org/10.1021/ja01269a023.

[64] E.A. Zaragoza-Contreras, C.A. Hernández-Escobar, A. Navarrete-Fontes, S. G. Flores-Gallardo, Synthesis of carbon black/polystyrene conductive nanocomposite. Pickering emulsion effect characterized by TEM, Micron 42 (2011) 263–270, https://doi.org/10.1016/j.micron.2010.10.005.

[65] K.R.V. Reddy, J. Keshavayya, Synthesis, magnetic, spectral, and thermal studies on metal(II) 1,3,8,10,15,17,22,24-octaaminophthalocyanines, Synthesis and Reactivity in Inorganic, Metal-Organic, Nano-Metal Chem. 32 (2002) 1235–1244, https://doi.org/10.1081/SIM-120014300.

[66] E.G. Ordoñez Casanova, F. Espinosa Magaña, A. Aguilar Elguezabal, Estudio experimental y teórico de nanotubos de carbono de pocas paredes, Centro de Investigación en Materiales Avanzados, 2013.

[67] K.S.W. Sing, Reporting physisorption data for gas/solid systems with special reference to the determination of surface area and porosity (Recommendations 1984), Pure Appl. Chem. 57 (1985) 603–619, https://doi.org/10.1351/pac198557040603.

[68] S.S. Batsanov, Van der Waals radii of elements, Inorg. Mater. 37 (2001) 871–885, https://doi.org/10.1023/A:1011625728803.

[69] D. Briggs, V.A. Gibson, Direct observation of multiplet splitting in 2P photoelectron peaks of cobalt complexes, Chem. Phys. Lett. 25 (1974) 493–496, https://doi.org/10.1016/0009-2614(74)85350-9.

[70] D.C. Frost, C.A. McDowell, I.S. Woolsey, X-ray photoelectron spectra of cobalt compounds, Mol. Phys. 27 (1974) 1473–1489, https://doi.org/10.1080/00268977400101251.

[71] M. Oku, X-ray photoelectron spectrum of low-spin Co(III) in $LiCoO_2$, J. Solid State Chem. 23 (1978) 177–185, https://doi.org/10.1016/0022-4596(78)90063-4.

[72] K. Chen, K. Liu, P. An, H. Li, Y. Lin, J. Hu, C. Jia, J. Fu, H. Li, H. Liu, Z. Lin, W. Li, J. Li, Y.-R. Lu, T.-S. Chan, N. Zhang, M. Liu, Iron phthalocyanine with coordination induced electronic localization to boost oxygen reduction reaction, Nat. Commun. 11 (2020) 4173, https://doi.org/10.1038/s41467-020-18062-y.

[73] R.A. Collins, K.A. Mohammed, Gas sensitivity of some metal phthalocyanines, J. Phys. D Appl. Phys. 21 (1988) 154–161, https://doi.org/10.1088/0022-3727/21/1/021.

[74] N.Sh Lebedeva, N.A. Pavlycheva, A.I. V'yugin, Kinetics of thermal oxidative decomposition of zinc porphyrin and phthalocyanine complexes, Russ. J. Gen. Chem. 77 (2007) 629–640, https://doi.org/10.1134/S1070363207040226.

[75] R. Seoudi, G.S. El-Bahy, Z.A. El Sayed, FTIR, TGA and DC electrical conductivity studies of phthalocyanine and its complexes, J. Mol. Struct. 753 (2005) 119–126, https://doi.org/10.1016/j.molstruc.2005.06.003.

[76] M. Viera, J. Riquelme, C. Aliaga, J.F. Marco, W. Orellana, J.H. Zagal, F. Tasca, Oxygen reduction reaction at penta-coordinated Co phthalocyanines, Front. Chem. 8 (2020) 1–12, https://doi.org/10.3389/fchem.2020.00022.

[77] J.J. Zagal, M. Páez, A.A. Tanaka, J.R. dos Santos, C.A. Linkous, Electrocatalytic activity of metal phthalocyanines for oxygen reduction, J. Electroanal. Chem. 339 (1992) 13–30, https://doi.org/10.1016/0022-0728(92)80442-7.

[78] A. Alsudairi, J. Li, N. Ramaswamy, S. Mukerjee, K.M. Abraham, Q. Jia, Resolving the iron phthalocyanine redox transitions for ORR catalysis in aqueous media,

J. Phys. Chem. Lett. 8 (2017) 2881–2886, https://doi.org/10.1021/acs.jpclett.7b01126.
[79] R. Chen, H. Li, D. Chu, G. Wang, Unraveling oxygen reduction reaction mechanisms on carbon-supported Fe-phthalocyanine and Co-phthalocyanine catalysts in alkaline solutions, J. Phys. Chem. C 113 (2009) 20689–20697, https://doi.org/10.1021/jp906408y.
[80] S. Baranton, C. Coutanceau, C. Roux, F. Hahn, J.-M. Léger, Oxygen reduction reaction in acid medium at iron phthalocyanine dispersed on high surface area carbon substrate: tolerance to methanol, stability and kinetics, J. Electroanal. Chem. 577 (2005) 223–234, https://doi.org/10.1016/j.jelechem.2004.11.034.
[81] Q. Zhao, Y. Wang, W.-H. Lai, F. Xiao, Y. Lyu, C. Liao, M. Shao, Approaching a high-rate and sustainable production of hydrogen peroxide: oxygen reduction on Co–N–C single-atom electrocatalysts in simulated seawater, Energy Environ. Sci. 14 (2021) 5444–5456, https://doi.org/10.1039/D1EE00878A.